



**HAL**  
open science

# Night-time Mesospheric/Lower Thermospheric Tropical Ozone Response to the 27-day Solar Rotational Cycle: ENVISAT-GOMOS Satellite Observations versus HAMMONIA Idealized Chemistry-Climate Model Simulations

Rémi Thiéblemont, Slimane Bekki, Marion Marchand, Sébastien Bossay, H. Schmidt, Mustapha Meftah, Alain Hauchecorne

## ► To cite this version:

Rémi Thiéblemont, Slimane Bekki, Marion Marchand, Sébastien Bossay, H. Schmidt, et al.. Night-time Mesospheric/Lower Thermospheric Tropical Ozone Response to the 27-day Solar Rotational Cycle: ENVISAT-GOMOS Satellite Observations versus HAMMONIA Idealized Chemistry-Climate Model Simulations. *Journal of Geophysical Research: Atmospheres*, 2018, 123 (16), pp.8883-8896. 10.1029/2017JD027789 . insu-01855666

**HAL Id: insu-01855666**

**<https://insu.hal.science/insu-01855666>**

Submitted on 3 Aug 2020

**HAL** is a multi-disciplinary open access archive for the deposit and dissemination of scientific research documents, whether they are published or not. The documents may come from teaching and research institutions in France or abroad, or from public or private research centers.

L'archive ouverte pluridisciplinaire **HAL**, est destinée au dépôt et à la diffusion de documents scientifiques de niveau recherche, publiés ou non, émanant des établissements d'enseignement et de recherche français ou étrangers, des laboratoires publics ou privés.

## RESEARCH ARTICLE

10.1029/2017JD027789

## Key Points:

- First observational estimate of the nighttime tropical O<sub>3</sub> response to the 27-day solar cycle in the mesosphere/lower thermosphere
- GOMOS observes a maximum absolute sensitivity of 1.8% change of ozone for 1% change in Lyman- $\alpha$  at 81 km
- HAMMONIA reproduces most of the features in the observed O<sub>3</sub> response to the 27-day solar cycle but underestimates its magnitude

## Correspondence to:

R. Thiéblemont,  
remi.thieblemont@latmos.ipsl.fr

## Citation:

Thiéblemont, R., Bekki, S., Marchand, M., Bossay, S., Schmidt, H., Meftah, M., & Hauchecorne, A. (2018). Nighttime mesospheric/lower thermospheric tropical ozone response to the 27-day solar rotational cycle: ENVISAT-GOMOS satellite observations versus HAMMONIA idealized chemistry-climate model simulations. *Journal of Geophysical Research: Atmospheres*, 123, 8883–8896. <https://doi.org/10.1029/2017JD027789>

Received 26 SEP 2017

Accepted 20 JUL 2018

Accepted article online 6 AUG 2018

Published online 27 AUG 2018

## Author Contributions:

**Conceptualization:** R. Thiéblemont, M. Marchand, S. Bossay

**Methodology:** R. Thiéblemont, S. Bekki, M. Marchand

**Formal analysis:** R. Thiéblemont

**Investigation:** R. Thiéblemont, S. Bekki, M. Marchand, M. Meftah

**Writing - original draft:** R. Thiéblemont, S. Bekki, S. Bossay

**Writing - review and editing:** R. Thiéblemont, S. Bekki, M. Marchand, H. Schmidt, M. Meftah, A. Hauchecorne

**Visualization:** R. Thiéblemont

**Supervision:** S. Bekki, M. Marchand, A. Hauchecorne

**Funding acquisition:** S. Bekki, A. Hauchecorne

**Validation:** H. Schmidt, M. Meftah, A. Hauchecorne

**Resources:** H. Schmidt, A. Hauchecorne

# Nighttime Mesospheric/Lower Thermospheric Tropical Ozone Response to the 27-Day Solar Rotational Cycle: ENVISAT-GOMOS Satellite Observations Versus HAMMONIA Idealized Chemistry-Climate Model Simulations

R. Thiéblemont<sup>1</sup> , S. Bekki<sup>1</sup>, M. Marchand<sup>1</sup>, S. Bossay<sup>1</sup>, H. Schmidt<sup>2</sup> , M. Meftah<sup>1</sup>, and A. Hauchecorne<sup>1</sup> 

<sup>1</sup>Laboratoire Atmosphères, Milieux, Observations Spatiales-IPSL, CNRS, Guyancourt, France, <sup>2</sup>Max-Planck-Institut für Meteorologie, Hamburg, Germany

**Abstract** Global Ozone Monitoring by Occultation of Stars (GOMOS) satellite data are analyzed to estimate the first observation-based nighttime (22:00 median local time) ozone response to the 27-day solar rotational cycle in the tropical mesosphere/lower thermosphere (50–110 km altitude). The ozone response to solar rotational variability is derived from linear correlation and regressions using Lyman- $\alpha$  line (121.6 nm) as solar index that varies by about 10–15% over solar rotational cycles. In the lower mesosphere (50–70 km), the GOMOS ozone is found to be correlated with the solar fluctuations and exhibits a sensitivity of  $\sim 0.1$  (expressed in percent change of ozone for 1% change in Lyman- $\alpha$ ). In the upper mesosphere/lower thermosphere (above 80 km), ozone variations become anticorrelated with solar rotational variations. In this region, the vertical profile of ozone sensitivity to the 27-day solar cycle exhibits a maximum of 1.8 at 81 km, a minimum of 0.3 at 100 km, and a sharp increase above. Such high ozone sensitivities are observed for the first time. The observed ozone response is compared with chemistry-climate simulations from the Hamburg model of the neutral and ionized atmosphere (HAMMONIA) that is forced with an idealized 27-day solar spectral irradiance time series. Although observational and model results share some common features, substantial discrepancies are found. Namely, the altitude of transition from positive to negative solar ozone correlation signal in the model simulation is found about 10 km below the altitude of the observations and the amplitude of the ozone sensitivity is generally vastly underestimated by the model.

## 1. Introduction

It is already well established that a substantial component of stratospheric ozone variability originates from short-term and long-term quasi-periodic fluctuations in solar activity, notably the 11-year solar magnetic activity cycle (also called the Schwabe cycle) and the 27-day solar rotational cycle (also called the Carrington cycle). Numerous observational (Bossay et al., 2015; Chandra & McPeters, 1994; Dikty et al., 2010; Fioletov, 2009; Hood, 1986; Hood & Zhou, 1998; Ruzmaikin et al., 2007; Zhou et al., 1997; Zhou et al., 2000) and modeling (Austin et al., 2007; Brasseur, 1993; Gruzdev et al., 2009; Merkel et al., 2011; Rozanov et al., 2006; Sukhodolov et al., 2017; Thiéblemont et al., 2017; Williams et al., 2001) studies have demonstrated the influence of the 27-day solar rotational cycle on stratospheric ozone. The main process responsible for the stratospheric ozone response to solar variability is the solar UV-driven photolysis of molecular oxygen (O<sub>2</sub>) that is the source of O<sub>3</sub> in the stratosphere. The effect of the 27-day solar rotational cycle on the mesosphere has attracted less attention. There have been quite a few modeling studies (e.g., Allen et al., 1984; Brasseur, 1993; Chen et al., 1997; Grenfell et al., 2010; Gruzdev et al., 2009; Kenesha et al., 1979; Rodrigo et al., 1981, 1986; Rozanov et al., 2006; Shimazaki & Laird, 1970; Sukhodolov et al., 2017), but the number of observational studies is very limited (Aikin & Smith, 1986; Eckman, 1986; Hood et al., 1991; Keating et al., 1987). One of the difficulties in detecting such a signal in the mesosphere is the considerable amplitude of the ozone diurnal variations (Brasseur & Solomon, 1986; Dikty et al., 2010; Huang et al., 2008; Vaughan, 1984). When a mesospheric ozone time series spans a range of local times varying from day to day (Smith et al., 2013), the short-term ozone variance can be vastly dominated by fluctuations associated with the sampling of the diurnal cycle. These fluctuations can be viewed as noise in the extraction of the solar signal and thus make uncertain the estimation of the ozone response to short-term solar variability.

The most suited mesospheric ozone data sets for detection is likely to be provided by Sun-synchronous satellites with measurements at nearly constant local times over the course of the mission. The SME (Solar Mesosphere Explorer) satellite, launched in a Sun-synchronous orbit, provides one of those data sets at fixed local time (Barth et al., 1983). To our best knowledge, it is the only observational data set that has been used successfully in the unambiguous detection of a solar rotational signal in mesospheric ozone. Aikin and Smith (1986) were the first to report conclusive evidence for solar rotational periodicities in mesospheric ozone time series with a significant correlation between ozone and a solar UV indicator, the Lyman- $\alpha$  line. They analyzed 244 days of SME ozone data, starting in January 1982, between 50 and 87 km, and found a significant correlation near 50 km and between 65 and 70 km. A correlation was also detected at higher altitudes between 80 and 85 km when only the first 110 days of data was considered. Keating et al. (1987) analyzed almost 2 years of SME data averaged between 40°N and 40°S and detected a maximum in ozone response near 0.05 mbar (70 km) with a peak ozone sensitivity value of  $-0.14$ , that is,  $-0.14\%$  ozone decrease for a 1% increase in solar Lyman- $\alpha$  line intensity (the Lyman- $\alpha$  line irradiance varies by about 10–15% over 27-day solar cycles). Finally, Hood et al. (1991) extended the analysis to about 4 years of SME data. Their results are generally in good agreement with Keating et al. (1987) with a peak negative ozone response near 70 km (corresponding to an ozone sensitivity of  $-0.16$  versus Lyman- $\alpha$  line and  $-0.65$  versus the solar 205-nm flux). They also detected a secondary maximum in the ozone response near 80 km. Interestingly, the altitude of this secondary maximum appears to correspond exactly to the altitude of the maximum in the mesospheric OH response to solar rotational variations (Shapiro et al., 2012). Shapiro et al. (2012) analyzed mesospheric OH and H<sub>2</sub>O data from Microwave Limb Sounder (MLS/Aura) on solar rotational time scales for two time periods corresponding to different phases of the 11-year cycle: from December 2004 to December 2005 (the period of *high activity* with a pronounced 27-day solar cycle) and from August 2008 to August 2009 (*solar minimum* period with a vague 27-day solar cycle). They demonstrated, for the first time, that mesospheric OH concentrations correlated well with the Lyman- $\alpha$  line intensity (correlation coefficients up to 0.79) at zero time lag. The OH response maximum was found at 80 km. At the same time, H<sub>2</sub>O is anticorrelated (correlation coefficients up to  $-0.74$ ) with the Lyman- $\alpha$  line intensity at nonzero time lag. The results confirm that mesospheric OH and H<sub>2</sub>O abundances are closely connected and that O<sub>3</sub> and solar irradiance are mostly anticorrelated in the mesosphere because of the Lyman- $\alpha$  line-driven photolysis of H<sub>2</sub>O that is a source of hydrogen radicals, the predominant ozone-destroying species at these altitudes.

In a modeling study using the chemistry-climate model Hamburg model of the neutral and ionized atmosphere (HAMMONIA), Gruzdev et al. (2009) compiled all these SME-derived results. They estimated ozone sensitivities as regression coefficients corresponding to maximum correlation (for varying time lags) instead of correlation at a null time lag. Model calculations were compared to observational results taking into account the strong diurnal ozone cycle. Daytime (local midday) ozone sensitivities and phases derived from the model calculations were found to be in reasonable agreement with the range of SME-derived values except for a maximum around 75 km where SME daytime observations indicated a much smaller sensitivity than the model. Model calculations also suggested that the ozone response to solar rotational variability was very strong in the upper mesosphere, especially for nighttime ozone. For instance, there was a very sharp increase in simulated (local midnight) ozone sensitivity above 75 km with sensitivity values exceeding 1.5% at night (ozone sensitivity with respect to a percent change in 205-nm solar flux). In contrast, simulated daytime sensitivity was peaking just below 80 km and falling back to half of the nighttime values in the upper mesosphere. SME data did not show a sharp increase in daytime ozone sensitivity in the upper mesosphere.

The purpose of the present study is to detect and characterize the response of mesospheric ozone observed by Environment Satellite (ENVISAT)-Global Ozone Monitoring by Occultation of Stars (GOMOS) to solar rotational variations. We focus on the analysis of the nighttime response and in the tropics because it is a region where the ozone response to solar variability is largely driven by photochemical processes, especially on solar rotational time scales. GOMOS covers the entire tropical mesosphere, up to  $\sim 110$  km, and provides measurements at nearly constant local times. GOMOS observational results are further compared with results from the HAMMONIA model, a chemistry-climate model (CCM) covering the middle atmosphere up to  $\sim 250$  km. This allows testing the ability of the model to simulate the mesospheric nighttime ozone response to solar rotational variations.

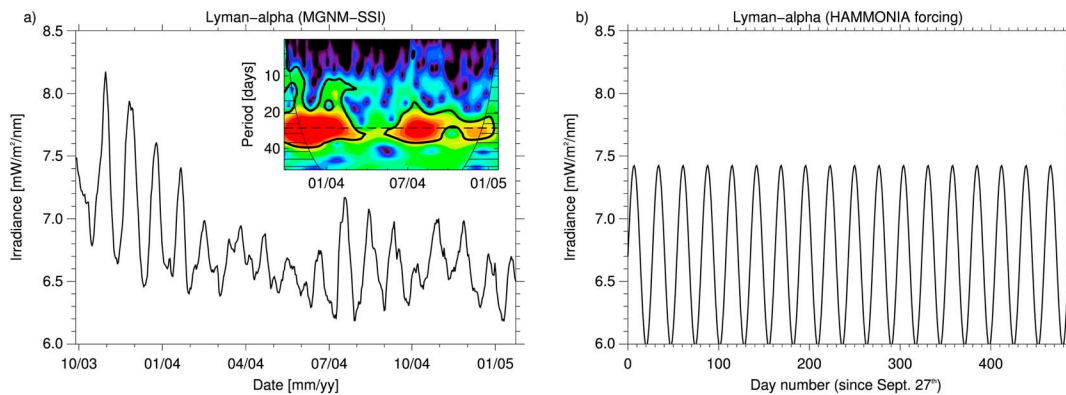


**Figure 1.** Time series of the daily Lyman- $\alpha$  spectral irradiance from (a) MGNM-SSI model and of (b) HAMMONIA solar forcing. The insert in Figure 1a shows the time-resolved power spectra densities of Lyman- $\alpha$  spectral irradiance estimated from continuous wavelet transform (CWT, Torrence & Compo, 1998). The black contour represents the 95% confidence level. HAMMONIA = Hamburg model of the neutral and ionized atmosphere; SSI = solar spectral irradiance.

## 2. Data and Methods

### 2.1. Solar Forcing

The Lyman- $\alpha$  line is chosen as the solar proxy because it determines the rate of H<sub>2</sub>O photolysis and hence the production of ozone-destroying hydrogen radicals, a key term in the mesospheric ozone chemical balance. Lyman- $\alpha$  line is also a general indicator of solar variability. The daily Lyman- $\alpha$  line time series is taken from the solar spectral irradiance (SSI) reconstruction model MGNM-SSI (Thuillier et al., 2012). It has been compared to the more commonly used Naval Research Laboratory-SSI model. SSI and its variability reconstructed by MGNM and Naval Research Laboratory were found to be consistent at the 5% level (Thuillier et al., 2014).

The HAMMONIA model was forced by a sinusoidal solar forcing  $S_{\lambda}$  with a period of 27 days that oscillates around the mean spectral solar flux  $S_{0,\lambda}$

$$S_{\lambda}(t) = S_{0,\lambda} + A_{\lambda} \sin(t/27)$$

where  $t$  is the time (in days) and  $A_{\lambda}$  is the wavelength-dependent amplitude of the irradiance as described in Gruzdev et al. (2009) that yields a variation of  $\sim 11\%$  for the Lyman- $\alpha$  line. This forcing design is certainly idealized since, in reality, the amplitude and period of the irradiance fluctuations associated with solar rotation varies in time. The phase of solar variations is also assumed to be independent of wavelength, which is a valid approximation for wavelengths shorter than 300 nm. As explained in Gruzdev et al. (2009), these simplifications aimed to reduce the degree of complexity in order to better identify the response to solar variations.

Figure 1 shows the solar irradiance forcing data used in our study. The Lyman- $\alpha$  line reconstructed in MGNM and its wavelet spectrum over the declining phase of solar cycle 23 (September 2003 to January 2005) are represented in Figure 1a. The magnitude of 27-day cycle is not constant in time, and its fluctuations are particularly pronounced over the subperiods September 2003 to February 2004 and June 2004 to November 2004. The wavelet spectrum further reveals that although the solar rotational cycle signal is centered around 27 days, it spans a rather broad of range periodicities from 20 to 35 days. This is due to the fact that active regions are not always located at the same longitude on the Sun and that the Sun's rotational period depends on the latitude (i.e., differential rotation). In comparison, the solar forcing used in HAMMONIA is periodic centered at 27 days and the amplitude of its variations is larger by a factor of  $\sim 1.5$  (Figure 1b).

### 2.2. Observations and Model Experiments

The ozone data used in our study are derived from the measurements made by the GOMOS instrument on board the European satellite ENVISAT. The GOMOS ozone data can be downloaded after registration at <http://earth.esa.int>. GOMOS provides ozone profiles from August 2002 to April 2012. Bertaux et al. (2010) give an overview of the GOMOS instrument, operation, data products, and scientific results. The measurement

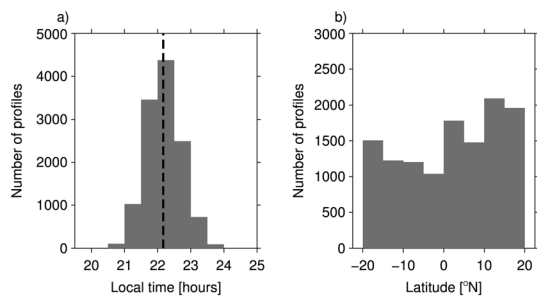


**Figure 2.** Distributions of the (a) local time and (b) latitude of the GOMOS ozone profiles selected over the period 27 September 2003 to 24 January 2005. GOMOS = Global Ozone Monitoring by Occultation of Stars.

technique is based on the stellar occultation by the Earth's atmosphere. The technique for determining ozone profiles from GOMOS observations is described by Kyrölä et al. (2006, 2010a, 2010b) and Sofieva et al. (2010). We use the Level 2 data from GOMOS products and follow recommendations from Kyrölä et al. (2006) in eliminating profiles from stars too cold ( $T < 7000$  K) or with a magnitude larger than 1.9. GOMOS ozone profiles, natively retrieved in number densities, are converted to volume mixing ratio (vmr) using Mass Spectrometer Incoherent Scatter (MSISE-90) temperature profiles (Hedin, 1991) that are provided with Level 2 GOMOS data for the mesosphere/lower thermosphere (MLT) region. The converted ozone spatial distribution and temporal variability are thus sensitive to uncertainties in temperature profiles. Potential impact on the ozone solar signals observed by GOMOS and their comparison with HAMMONIA results will be discussed in section 4.

GOMOS suffered a serious electronic malfunction of the mirror steering mechanism from January 2005 to August 2005 leading to a shut down for several months. Other periods with large gaps occurred before (e.g., several gaps from May to September 2003) and later (especially in 2009), reducing the number of profiles available. In order to limit the impact of these large periods without data, we only consider the period September 27 2003 to 24 January 2005 (486 days or  $\sim 17$  solar rotational cycles) that is characterized by a weak percentage (8%) of days with missing data (after eliminating invalid profiles as described above). Indeed, if we considered the whole period (2002–2012), about 38% of days with ozone data are missing in the altitude range of interest. We further notice that the years 2006–2011 were characterized by an anomalously extended period of quiet Sun conditions associated with very low amplitudes of the SSI fluctuations at 27-day solar rotational time scales, making this period inappropriate for our study. Above 105 km, the accuracy of retrievals drops and the percentage of missing data increases dramatically.

In this study, we only consider GOMOS dark limb measurements, that is, with the solar zenith angle at the tangent point greater than  $107^\circ$ . GOMOS is able to measure using stars outside the Sun-synchronous orbital plane of ENVISAT that leads to variations in the local hour of measurements. Figure 2 shows the distribution of the (a) local hour and (b) latitude of all profiles selected for our study (13,957 in total) in the latitude range  $20^\circ\text{S}$ – $20^\circ\text{N}$ . GOMOS profile local times are comprised namely between 21:00 and 23:30 with a median value near 22:00 corresponding to the crossing time of the equator along the orbit of ENVISAT (Figure 2a). Although ozone profiles cover all latitudes in the range  $20^\circ\text{S}$ – $20^\circ\text{N}$ , they are not evenly distributed; 59% are sampled in the Northern Hemisphere. The profiles extend up to 150 km and have a vertical resolution in the mesosphere of 3 km. Finally, daily mean ozone profiles are obtained by calculating the mean of the selected ozone profiles for each day of the period 27/09/2003–24/01/2005. Note that on average, daily mean profiles are calculated from 14 individual profiles; less than 2% of the daily mean profiles (i.e., 8 in total) are calculated from less than 4 individual profiles.

GOMOS observational results are compared with the results of HAMMONIA model experiments that are detailed in Gruzdev et al. (2009). A comprehensive description of the model is given in Schmidt et al. (2006). In brief, HAMMONIA is a global three-dimensional chemistry-climate model extending from the surface to the thermosphere with a lid height at about 250 km. HAMMONIA is an extension toward higher altitudes of the ECHAM5 (Roeckner et al., 2003, 2006) and MAECHAM5 (Giorgetta et al., 2006; Manzini et al., 2006) general circulation models, interactively coupled with the Model for Ozone And Related chemical Tracers (MOZART3) chemistry scheme (Kinnison et al., 2007). The model is run with a spectral truncation of T31 (corresponding approximately to a horizontal resolution of  $3.75 \times 3.75^\circ$ ) with 67 vertical levels. In this version, HAMMONIA describes 48 chemical species with 46 photolysis and 107 bimolecular and termolecular gas phase reactions (see Tables 1 and 2 in Schmidt et al., 2006). The photolysis rates are calculated as a function of geopotential height, surface albedo, ozone column, and solar zenith angle using the Tropospheric and Ultraviolet Visible radiative model (Madronich & Flocke, 1999) with 122 wavelength bands over the 200 to 780-nm interval. From 120 to 200 nm, the spectrum is treated with 34 wavelength bands and uses parameterizations for the photolysis of  $\text{O}_2$  from Chabrilat and Kockarts (1998; Lyman- $\alpha$ ), Brasseur and Solomon (1986; Schumann-Runge continuum), and Koppers and Murtagh (1996; Schumann-Runge bands). The NO photolysis is treated according to Minschwaner and Siskind (1993).

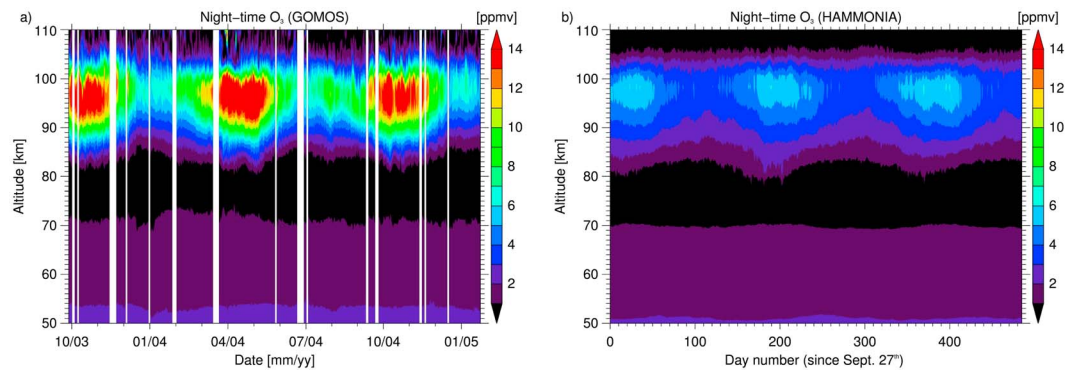


**Figure 3.** Daily nighttime tropical mesospheric ozone (a) measured by ENVISAT GOMOS over the declining phase of solar cycle 23 (September 2003 to January 2005) and (b) simulated by HAMMONIA. White areas indicate days with missing or excluded data. ENVISAT = Environment Satellite; GOMOS = Global Ozone Monitoring by Occultation of Stars; HAMMONIA = Hamburg model of the neutral and ionized atmosphere.

Two HAMMONIA free-running simulations are analyzed in our study. The simulation used for comparison with observational results is forced with the idealized periodic solar forcing shown in Figure 1b. Except for the 27-day variation of solar irradiance, all boundary conditions are kept constant (i.e., upper and lower boundary source gas concentrations, with values typical for the 1990s as, for example, a  $\text{CO}_2$  mixing ratio of 360 ppm) or prescribed with an annually repeating seasonal cycle (i.e., SSTs and sea ice). The solar irradiance varies around mean values taken from an average for the first 6 months of 1990, that is, conditions near to a solar maximum and similar to the years 2003–2005. In addition, we use the simulation without 27-day solar fluctuations also described in Gruzdev et al. (2009). Analysis of this constant forcing simulation aims to assess the robustness of the solar signals derived from the periodically forced simulation (see section 2.3). Both simulations were performed over 6 years of which only the last 5 years are analyzed. HAMMONIA daily averaged tropical ozone profile are derived by computing the average of all profiles in the latitude range  $20^\circ\text{S}$ – $20^\circ\text{N}$  and in the local time range 21:00–24:00 for each day of the simulations, in order to mimic the GOMOS sampling. Note that we repeated all the analysis of our study by restricting the HAMMONIA local time range sampling to 21:30–22:30, but the differences in the results were found to be insignificant.

The temporal evolution of the observed (GOMOS) and simulated (HAMMONIA) mesospheric nighttime ozone profiles (between 50 and 110 km) are shown in Figures 3a and 3b, respectively. To facilitate the comparison with GOMOS, ozone from HAMMONIA is shown over a 486-day period that starts on 27 September. GOMOS ozone mixing ratio peaks in the mesopause region (around 95 km) at values higher than 15 ppm (Figure 3a). This secondary ozone maximum (as compared to the original stratospheric ozone maximum) results from the combined effects of the atomic oxygen maximum at the mesopause and the prevailing very low temperature that affect chemical rate coefficients and atmospheric density (Smith & Marsh, 2005). Above 80 km, there is a very clear semiannual oscillation signal marked by the highest ozone values seen around the equinox times, when the diurnal tide amplitude is largest (Pancheva et al., 2014; Smith et al., 2008). Using a migrating diurnal tide model, Smith et al. (2008) demonstrated that the associated upward motions cool the air adiabatically and bring low concentrations of atomic oxygen and hydrogen from below. The net effect is a much higher equilibrium ozone values, mainly caused by the strongly reduced temperatures. In HAMMONIA, very similar features are found but the secondary ozone maximum near 95 km and the magnitude of the relative variations of its semiannual oscillation are reduced by a factor of 2 compared to GOMOS observations (Figure 3b). Schmidt et al. (2006) already noticed an underestimation of the ozone secondary maximum in HAMMONIA compared to Sounding of the Atmosphere using Broadband Emission Radiometry observations during daytime. Similarly, Smith et al. (2015) found that the Whole Atmosphere Community Climate Model simulated  $\text{O}_3$  near the mesopause region that was about 50% lower than observed by Sounding of the Atmosphere using Broadband Emission Radiometry. They related this underestimation of ozone in the model to an underestimation of atomic oxygen that is itself strongly influenced by effective transport due to eddy and molecular diffusive processes that are parameterized in the Whole Atmosphere Community Climate

Model and HAMMONIA. An underestimation of downward mixing of atomic oxygen is also a likely cause for the underestimation of ozone seen in HAMMONIA.

### 2.3. Analytical Methods

The ozone response to the solar rotational cycle is derived from linear correlation and regression techniques using the Lyman- $\alpha$  line as predictor. Time series are primarily band-pass filtered in order to focus on the solar rotational periodicities. The filtering procedure consists of first applying a 7-day running mean to remove short-term fluctuations. A 35-day running mean is then subtracted from the data to remove long-term fluctuations (e.g., seasonal, semiannual, annual, and quasi-biennial oscillations).

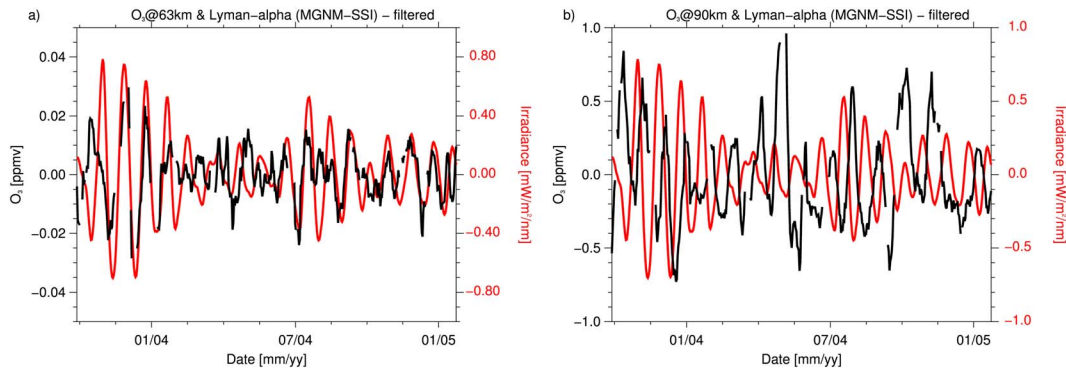
Given the high degree of serial correlation in band-pass filtered time series, the statistical significance of correlation coefficients between ozone and the Lyman- $\alpha$  flux is derived from a nonparametric random phase test that accounts for autocorrelation in time series (Ebisuzaki, 1997). In practice, we generate synthetic random time series with the same power spectra as the original filtered ozone time series but with random phases in the Fourier modes. Then, the correlation coefficient between the synthetic random time series and the Lyman- $\alpha$  flux is calculated. This procedure is repeated 1,000 times, and the derived correlation coefficients are then used to construct a probability distribution of correlation coefficients from which two-sided 90%, 95%, and 99% confidence limits are determined. Note that we also tested the Cholesky decomposition method, described by Haam and Tung (2012), to generate randomized time series. The tests that we carried out gave results similar to those obtained with the random phase method. Yet we did not opt for the Cholesky decomposition method as it happened to be significantly more computationally demanding. To assess the statistical significance of correlation coefficients in the model, we additionally use the constant forcing HAMMONIA experiment to estimate the probability distribution of spurious significant correlations (details are provided in section 3).

The ozone response to changes in Lyman- $\alpha$  is presented in terms of sensitivity, that is, percentage change in ozone per 1% change in Lyman- $\alpha$ . The ozone sensitivity is simply derived by regressing the filtered ozone time series on the Lyman- $\alpha$  flux. As pointed out above, the filtering procedure of the time series leads to serially correlated residuals which, if not accounted for, can lead to an underestimation of the standard error on the regression coefficients. We hence derive the standard error using a block bootstrapping technique as described hereafter (Mudelsee, 2014). The initial residuals are first obtained by subtracting the original fitted model (i.e., derived from the linear regression) to the dependent variable. These initial residuals are then segregated into moving blocks of length  $L$  (see, e.g., schematic p74 in Mudelsee, 2014) that are randomly resampled to reconstruct synthetic residuals of the same size as the initial ones. Adding these synthetic residuals to the original fitted model allows creating a randomized time series (so-called bootstrap sample) to which the linear regression is applied to derive a synthetic regression coefficient value. This procedure is repeated 1,000 times, which allows constructing a probability distribution of regression coefficients used then to determine the confidence intervals. Note that since  $L$  is not known a priori, the block bootstrapping method is repeated for  $L = 1, 2, 3, \dots, 10, \dots, 20$ , etc. until confidence intervals become stable. Typically, stable confidence intervals are found for  $L \geq 20$ .

## 3. Results

### 3.1. Detecting the Ozone Response the 27-Day Solar Cycle

Figure 4 shows the digitally filtered time series of the observed Lyman- $\alpha$  line irradiance and mesospheric ozone. At 63 km (Figure 4a) the Lyman- $\alpha$  and ozone time series appear to be overall positively correlated with a correlation coefficient of 0.44 ( $p < 0.05$ ) between the two time series. The correlation coefficient value is maximum (0.46) when the Lyman- $\alpha$  line lags the ozone time series by 1 day (i.e., lag of  $-1$  day). We additionally carry out a cross-spectrum analysis of Lyman- $\alpha$  and ozone time series that revealed a significant and in-phase spectral coherency at 27-day solar time scales (not shown). Note that the correlation seems particularly pronounced for periods when the amplitude of the 27-day cycle is largest (around January and July 2004). At 90 km (Figure 4b), inversely, the solar forcing and the ozone time series are overall anticorrelated with a correlation coefficient of  $-0.33$  at lag 0 that maximizes at lag  $-4$  days with a value of  $-0.49$  ( $p < 0.05$ ). The anticorrelation is easier to distinguish over the months around January 2004 and after July 2004.



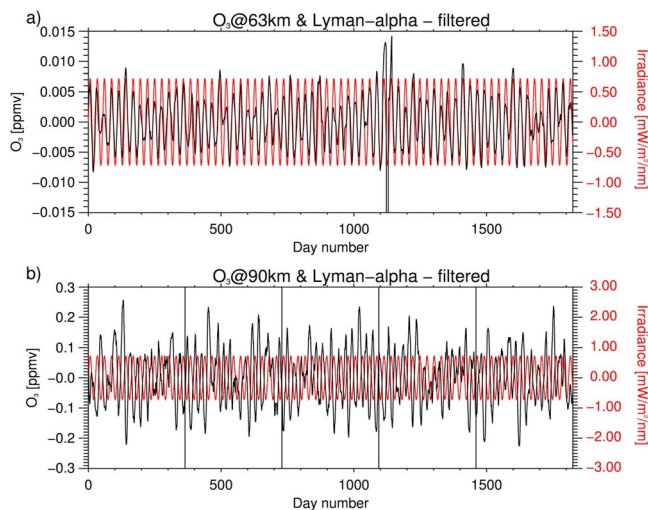
**Figure 4.** Temporal evolution of anomalies of (red) Lyman- $\alpha$  line and (black) ozone measured by GOMOS at (a) 63 km and (b) 90 km. The time series have been digitally filtered (see section 2.3 for details). SSI = solar spectral irradiance; GOMOS = Global Ozone Monitoring by Occultation of Stars.

Figure 5 shows an analogous analysis of the Lyman- $\alpha$ /ozone time series for the model data from the simulation with the periodic solar forcing. In the lower mesosphere (at 63 km, Figure 5a), the simulated ozone oscillates in phase with the solar forcing at 27-day time scales with a maximum correlation coefficient of 0.76 at lag 0 ( $p < 0.05$ ). This appears qualitatively consistent with the observational results (Figure 4a), although the maximum correlation coefficient is much larger in the model simulation. Note also that the amplitude of the simulated ozone fluctuations is smaller than in the observations despite the stronger amplitude of the solar forcing in the model. In the upper MLT (at 90 km, Figure 5b), the simulated ozone oscillates out of phase with the solar forcing with a minimum correlation coefficient of  $-0.69$  ( $p < 0.05$ ) at a lag of 1 day. Overall, although the model results share common features with the observational results (Figure 4b), significant differences are found: (i) the amplitude of the simulated ozone fluctuations (smaller in the model), (ii) the magnitude of the correlation coefficient (larger in the model), and (iii) the lag of the minimum correlation that differs by 5 days.

Although the correlation coefficients derived from the cross analysis of the Lyman- $\alpha$  line and the ozone time series reported above are statistically significant according to the nonparametric test (see section 2.3), we additionally test the robustness of ozone/Lyman- $\alpha$  relationship using the constant forcing (i.e., no solar fluctuations) simulation. We apply the same filtering procedure to the ozone time series from the constant solar forcing simulation and correlate it with the periodical and observed solar forcing in order to estimate

the likelihood to obtain spurious correlations as a function of the length of the time window of analysis. The procedure is as follows: a segment of the periodical Lyman- $\alpha$  time series of a given length is selected (in the range [50, 1700] days) and slid by increment of 1 day until the full filtered ozone time series has been scanned. For each time increment, the correlation coefficient between the Lyman- $\alpha$  and the filtered ozone time series is calculated. This allows constructing a probability distribution of spurious correlation coefficients for each time window length considered.

Figure 6 shows the two-sided 90, 95, and 99% confidence intervals of the spurious correlation coefficients probability distribution derived at 63 km. As expected, the chance to obtain a spurious correlation is high when a (very short) 50-day time window is considered as shown by the 95% confidence interval comprised between  $-0.75$  and  $0.75$ . The 95% confidence interval rapidly narrows with increasing time window length and stabilizes close to  $[-0.2, 0.2]$  when the length of the time window exceeds 1,000 days. This confirms the soundness of the correlation found between ozone and solar variability in the periodically forced simulation (Figure 5). Thereafter, the confidence limits determined here and for all altitude levels of the model (not shown) will be used to assess further the statistical significance of the Lyman- $\alpha$ /ozone correlation coefficients obtained from the model results. Near 486 days—corresponding to the



**Figure 5.** Temporal evolution of anomalies of (red) Lyman- $\alpha$  line and (black) ozone simulated by periodically forced HAMMONIA experiment at (a) 63-km and (b) 90-km altitudes. The time series have been digitally filtered. HAMMONIA = Hamburg model of the neutral and ionized atmosphere.

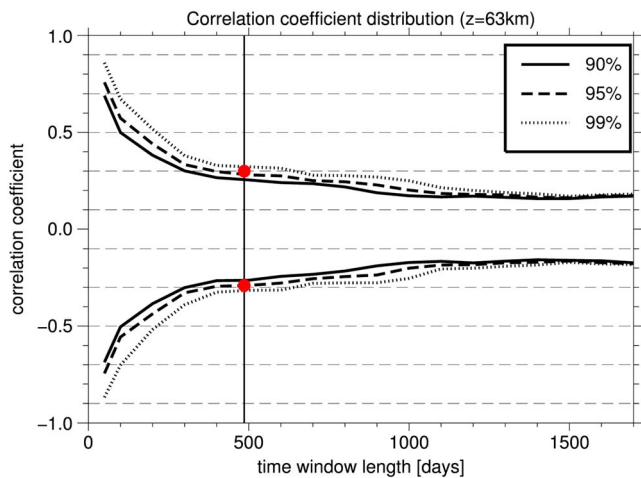
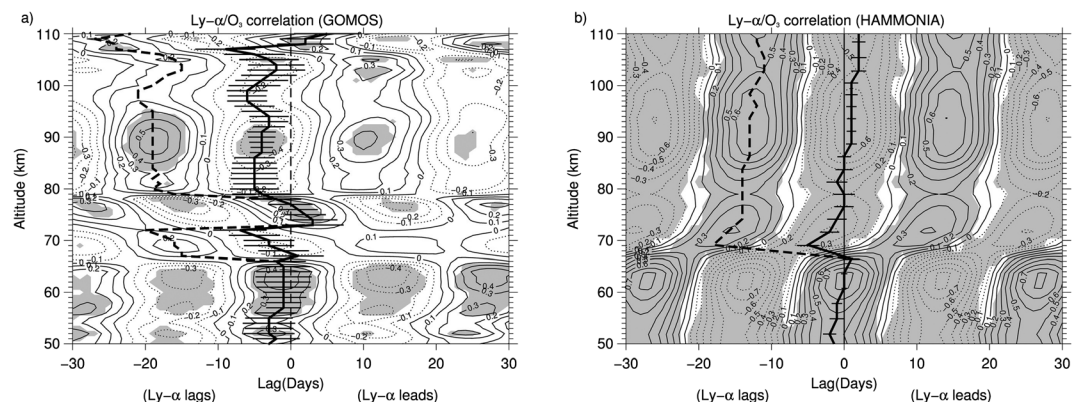


**Figure 6.** Two-sided 90 (solid), 95 (dashed), and 99% (dotted) tails of the distribution of correlation coefficients between the periodical solar forcing and the ozone time series of the constant forcing (i.e., no solar fluctuations) simulation. The distribution is plotted as a function of the length of the time window of analysis. The two red dots mark the two-sided 95% confidence limits calculated from the observed solar forcing instead of the periodical solar forcing and over a time window of a length of the observed period (i.e., 486 days).

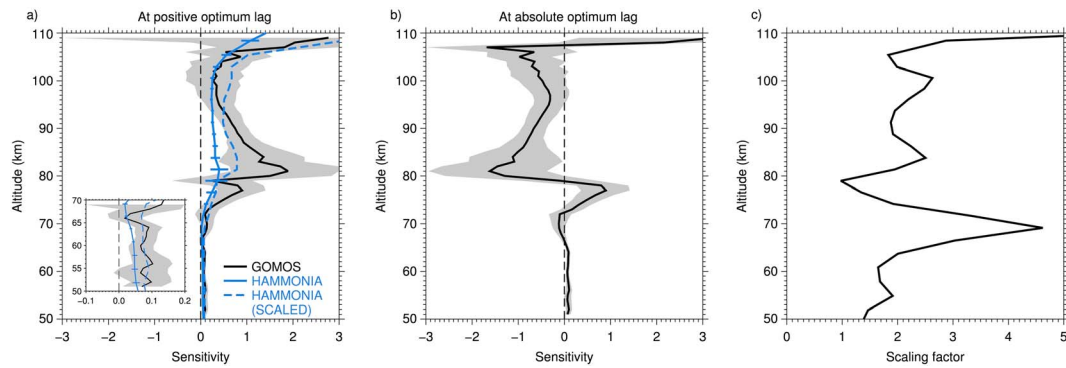
length of the observed period—the 95% confidence interval is  $[-0.3, 0.3]$  when considering either the periodical solar forcing (dashed line) or the observed MGNM-SSI forcing (red dots). This confidence interval supports the fact that the maximum correlation coefficients derived from observations (i.e., Figures 4, 0.46 at 63 km and  $-0.49$  at 90 km) are not spurious. Note that this intends to be illustrative only since the simulated ozone time series (upon which the confidence intervals are calculated) differ from the observed ones.

Figure 7 shows the lead-lag correlation coefficients between Lyman- $\alpha$  line for GOMOS and HAMMONIA as a function of altitude in the MLT region. Lead-lag correlations are estimated over the entire time series, that is, 486 days for the observations (Figure 7a) and 1,826 days for the model (Figure 7b). Negative (positive) lag values indicate that the solar forcing lags (leads) the ozone response, respectively. The observations and the model results share some consistent features in sign above 80 km and below 70 km. As expected from the time series analysis (i.e., Figures 4 and 5), positive correlations are found in the lower mesosphere near zero time lag and negative correlations in the upper MLT. The altitudes of maximum correlation are also consistently found close to 63 and 90 km in both observations and model results. Note that the correlation coefficients are larger for the model results though. This is partly due to the idealized and stronger solar irradiance 27-day amplitude used to force the model. In the upper stratosphere/lower mesosphere, the positive

correlation between the solar forcing and ozone originates in the increased photolysis of the molecular oxygen (in the Schuman-Runge bands and Herzberg continuum) associated with increased solar irradiance, which in turn results in positive ozone changes. Above 65 km, the role of hydrogen radicals—whose concentration increases with Lyman- $\alpha$  intensity (through photolysis of  $H_2O$ )—becomes prominent and reduces the ozone concentration (Brasseur, 1993; Chen et al., 1997; Fleming et al., 1995; Shapiro et al., 2012). This effect increases with height and is consistent with the negative correlation between solar forcing and ozone found in the upper mesosphere near zero time lag. Above the mesopause ( $\sim 95$  km), the temperature responds significantly and positively to the 27-day solar variations (see also Gruzdev et al., 2009) and can therefore also contribute to the negative ozone response (due to the temperature dependence of the ozone photochemical equilibrium).



**Figure 7.** Lead-lag correlations between filtered ozone and Lyman- $\alpha$  spectral irradiance as a function of time lag (days) and altitude (km) for (a) GOMOS and (b) HAMMONIA. The shading indicates that correlation coefficients are statistically significant at the 95% confidence level. The dashed line indicates the vertical profile of the lag corresponding to the maximum positive correlation (or positive optimum lag), and the solid line indicates the vertical profile of the lag corresponding to the maximum absolute correlation nearest zero lag (or absolute optimum lag). Horizontal bars correspond to the  $2\text{-}\sigma$  confidence intervals (see text for details). GOMOS = Global Ozone Monitoring by Occultation of Stars; HAMMONIA = Hamburg model of the neutral and ionized atmosphere.



**Figure 8.** Mean ozone sensitivity profile to Lyman- $\alpha$  line (% change in ozone for 1% change in Lyman- $\alpha$ ) at (a) positive optimum and (b) absolute optimum lag for GOMOS (black line) and HAMMONIA (blue line). The gray shading and blue error bars delimit the 95% confidence interval of the ozone sensitivity estimates (see section 2.3) for GOMOS and HAMMONIA, respectively. In Figure 8a, the dashed HAMMONIA profile has been corrected by the scaling factor shown in Figure 8c. See text for details. GOMOS = Global Ozone Monitoring by Occultation of Stars; HAMMONIA = Hamburg model of the neutral and ionized atmosphere.

The largest discrepancies between GOMOS and model results are found in the altitude range 67–80 km. In this region, the correlations are barely significant in the observations and particularly weak in the model (lower than 0.4). Recall that the 70–80 km altitude range corresponds to the minimum in the mesospheric ozone profile (see Figures 3a and 3b) with mixing ratios of less than 0.5 ppmv. As a result, GOMOS measurement relative errors peak in this region, which makes the uncertainties on the derived signals larger. Finally, in the altitude range 65–80 km, the net ozone response to 27-day solar rotational cycle results mainly from the balance between two effects. An increase in solar irradiance leads to increased ozone production from the enhanced photolysis of the molecular oxygen in the Schumann-Runge range and increased ozone destruction from the enhanced photodissociation of water vapor by Lyman- $\alpha$  that produces HO<sub>x</sub> radicals. The competing influence of both effects on ozone may further contribute to the difficulty of identifying the 27-day solar signal, particularly given the relatively short observed time series.

Figure 7 also shows the vertical profiles of the lag corresponding to the maximum positive correlation (called positive optimum lag, dashed line) and of the lag corresponding to the maximum absolute correlation nearest zero lag (hereafter called absolute optimum lag, solid line). The uncertainties on the optimum lag are estimated by calculating, for each 27-day cycle, the deviation between the local absolute optimum lag and the average absolute optimum lag (i.e., calculated from all the 27-day cycles), from which we then infer confidence intervals. In the observations (Figure 7a), below 66 km, the optimum lag is included in the range –1 to –3 days that is consistent with the model results (Figure 7b) and previous observational results (e.g., SME satellite results in Hood et al., 1991). Above 80 km, the observed optimum lag fluctuates around –20 days but appears stable at –19 days in the range 85–95 km, where correlations are significant (Figure 7a). In comparison, the optimum lag tilts with height in the model (from –14 days at 80 km to –12 days at 110 km) and shows a significant difference of ~5 days with the observations in the range 85–95 km (Figure 7b).

### 3.2. Ozone Sensitivity to the 27-Day Solar Cycle

Figure 8 shows the ozone sensitivity calculated at positive optimum lag (Figure 8a) and absolute optimum lag (Figure 8b) over the entire time series. In the lower mesosphere (below 70 km, see zoom in Figure 8a), the observed ozone sensitivity profile (black line) shows small and nearly constant values (0.1). These values are consistent with those found in SME observations (Hood et al., 1991). The GOMOS ozone sensitivity profile at positive optimum lag exhibits a secondary maximum of 1.8 at 81 km followed by a secondary minimum at higher altitude (0.3 at 100 km). The standard error estimate is particularly large near 80 km that is consistent with the peak of GOMOS measurement relative errors as mentioned previously. A sharp increase of ozone sensitivity is then observed up to 110 km where a sensitivity value close to 3.0 is reached. Note, however, that the standard error estimate of the ozone sensitivity considerably increases above 105 km, consistent with the drastic drop in the accuracy of the ozone retrieval at these altitudes. To our knowledge, it is the first time that such an extended profile (above 80 km) of ozone sensitivity to solar rotational cycle is derived from an observational data set. The comparison of the ozone sensitivity profiles at positive (Figure 8a) and absolute

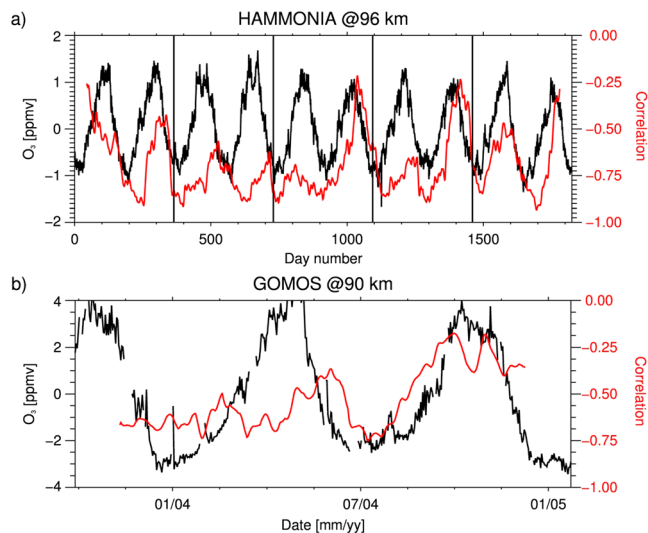


**Figure 9.** Temporal evolution of the unfiltered ozone anomalies (in black) and of the sliding correlation coefficients (in red, see text for details) between the filtered ozone and the Lyman- $\alpha$  line time series for (a) the model at 96 km and (b) the observations at 90 km. GOMOS = Global Ozone Monitoring by Occultation of Stars; HAMMONIA = Hamburg model of the neutral and ionized atmosphere.

(Figure 8b) optimum lag shows a clear symmetry about the y axis above 80 km. The secondary minimum of  $-1.8$  at 81 km (Figure 8b), where ozone variations are nearly out of phase with the Lyman- $\alpha$  (see Figure 7), coincides with the maximum OH response to Lyman- $\alpha$  observed in Aura MLS satellite data (Shapiro et al., 2012).

The profile of ozone sensitivity to solar forcing calculated over 5 years of HAMMONIA simulation is shown in blue (Figure 8a). The HAMMONIA sensitivity values compare well with those derived from Solar Climate Ozone Links (SOCOL) model simulations, as shown in Rozanov et al. (2006, see their Figure 7) or Sukhodolov et al. (2017, see their Figure 7) for the low mesosphere. In both studies, they found an ozone sensitivity of  $\sim 0.3$  (calculated as percent change in ozone for 1% change in irradiance flux at 205 nm) below 65 km, which is consistent with the ozone sensitivity of  $\sim 0.06$  (with respect to 1% change in the Lyman- $\alpha$ ) found in HAMMONIA. Indeed, the amplitude of the Lyman- $\alpha$  line fluctuations is 4 to 5 times larger than irradiance fluctuations at 205 nm. From  $\sim 70$  to 80 km, the sharpness of the ozone sensitivity increase is also consistent between Socol and HAMMONIA.

The shape of the sensitivity profile in HAMMONIA is qualitatively similar to results obtained with GOMOS observations, featuring low values ( $< 0.1$ ) that decrease with height below 70 km, a secondary maximum at 82 km, and a sharp increase between 100 and 110 km altitude. Quantitatively,

the ozone sensitivity appears to be globally underestimated in the model compared to the observations. In the lower mesosphere (below 70 km), the simulated ozone sensitivity is however close to the lower limit of the confidence interval of the observational results and even well within this interval in the thermosphere (above 95 km). The underestimation is particularly pronounced in the altitude range of the secondary maxima (70–95 km). As already noticed (e.g., Figures 3–5), substantial differences are found in climatological ozone mean mixing ratio and variability between GOMOS and HAMMONIA. To somewhat account for these differences in the comparison between GOMOS and HAMMONIA, we scale the HAMMONIA ozone sensitivity profile by multiplying, for each altitude, the sensitivity by the ratio between the relative variability of ozone in GOMOS and the relative variability of ozone in HAMMONIA (the relative variability is defined as the ratio between the standard deviation and the mean of a time series). The vertical profile of the scaling factor is shown in Figure 8c. After this scaling, the entire scaled HAMMONIA ozone sensitivity profile lies within the uncertainty range of the estimated GOMOS ozone sensitivity profile and shows a particularly good agreement with the model in the lower mesosphere (see zoom in Figure 8a).

### 3.3. Influence of the Semiannual Oscillation on the Ozone Solar Signal

Finally, we examine whether the semiannual oscillation of ozone (which maximizes in the mesopause region, see Figure 3) has an influence on the relationship between the solar forcing and the ozone temporal evolution. Figure 9 shows the unfiltered ozone anomaly for the model at 96 km (Figure 9a) and observations at 90 km (Figure 9b) from which we can easily identify the semiannual oscillation that largely dominates the variability. Note that these altitudes correspond to the upper mesosphere level where the largest negative correlation between filtered Lyman- $\alpha$  and ozone time series is found (see Figure 7). The red curve indicates the sliding correlation at absolute optimum lag between the Lyman- $\alpha$  and the filtered ozone time series (i.e., between curves shown in the same panels of Figures 4 or 5). The sliding correlation coefficient is calculated using a 90-day running time window, that is, spanning slightly more than three solar rotational cycles.

As expected, the solar forcing and ozone are anticorrelated over the whole period in both the model and observations (Figure 9). However, the correlation coefficient value is not constant. In the model (Figure 9a), it appears to be paced with the semiannual oscillation with the local anticorrelation maxima (i.e., highest negative values) generally occurring  $\sim 25$  days after the minimum phases of the semiannual oscillation. Reciprocally, the local anticorrelation minima (i.e., lowest negative values) follow maximum phases of the semiannual oscillation. Likewise, the analysis of the ozone sensitivity revealed that the maximum absolute

sensitivity coincides with minimum phases of the ozone semiannual oscillation with a lag of  $\sim 3$  weeks (not shown). In contrast, in the observations (Figure 9b), no clear relationship can be identified visually. We found that the anticorrelation maximizes  $\sim 22$  days after the minimum phases of the semiannual oscillation, which is consistent with the model results. However, the relationship is not statistically significant ( $p > 0.1$ ). This might be partly due to the time-dependent forcing and the relatively short observational period that both make the detection of an anticorrelation modulation by the semiannual oscillation difficult.

#### 4. Summary and Discussion

In this study, we present a new observational analysis of the response of mesospheric tropical ozone to the solar rotational cycle whose main periodicity is around 27 days. We use the GOMOS ozone measurements around 22:00 median local time that covers the entire mesosphere and lower thermosphere. It is of interest to consider the nighttime ozone sensitivity because chemistry-climate model calculations suggested that the strongest response to solar rotational variability occurs during the nighttime in the upper mesosphere (Gruzdev et al., 2009). The GOMOS measurement characteristics are well suited to test these model predictions. The Lyman- $\alpha$  line is chosen as the solar proxy because it determines the rate of  $\text{H}_2\text{O}$  photolysis and hence the production of ozone-destroying hydrogen radicals ( $\text{HO}_x$ ), a key term in the mesospheric ozone chemical balance. The 486-day period of GOMOS measurements considered here falls into the descending phase of the 11-year solar cycle 23.

GOMOS ozone nighttime data show a positive correlation with the solar forcing in the lower mesosphere and an anticorrelation in the upper mesosphere. These results are consistent with the prominent effect of increased molecular oxygen photodissociation with increased solar UV in the lower mesosphere (leading to enhanced ozone production and hence positive anomalies), which, with height, is progressively countered by enhanced  $\text{HO}_x$  radical production through increased  $\text{H}_2\text{O}$  photodissociation (leading to negative ozone anomalies). A very sharp height transition between positive and negative correlations is found at 80 km. The time lag of absolute optimum solar ozone correlation is found between  $-1$  and  $-3$  days in the lower mesosphere (below 70 km) and at  $-19$  days above 80 km. The observed ozone sensitivity vertical profile at maximum time lag shows a secondary maximum of 1.8 at 81 km and a strong increase above 100 km. These sensitivity values obtained from GOMOS nighttime observations demonstrate the strongly enhanced ozone response to the solar rotational cycle in the upper mesosphere compared to the daytime results obtained from SME (Hood et al., 1991; Keating et al., 1987). This supports the modeling-based findings of Gruzdev et al. (2009).

Although GOMOS observational results and HAMMONIA-based results share some common features, significant discrepancies are identified. For instance, the altitude of transition from positive to negative solar ozone correlation in the model simulation is found about 10 km below the altitude of the observations (i.e., 70 km instead of 80 km). The region located between 70 and 80 km altitude corresponds to a layer with a very low ozone content (lower than 0.5 ppm) with large relative observation errors, where the  $\text{HO}_x$  influence in destroying ozone becomes prominent (e.g., Chen et al., 1997). The solar signal in ozone in this layer may hence be difficult to identify, particularly with regard to the relatively short period of observations. The timing of the ozone response to 27-day fluctuations in the upper mesosphere also slightly differs between the model and the observations with a difference of  $\sim 5$  days around 90 km. More importantly, the observations/model comparison reveals large differences in the ozone sensitivity values. Although the shape of the ozone sensitivity vertical profile in the model is qualitatively consistent with the profile derived from observations (i.e., secondary maximum near 82-km altitude and strong increase above 100 km), ozone is much less sensitive to solar fluctuations in the model than observed by GOMOS.

One possible cause for the discrepancies between observations and model simulations is model biases in the representation of processes that control the ozone response to solar irradiance fluctuations. For instance, we computed the daytime OH sensitivity to the 27-day variations in HAMMONIA and it appeared to be underestimated compared to the OH sensitivity derived from MLS data by Shapiro et al. (2012). This may be indicative of an underestimation of  $\text{H}_2\text{O}$  photodissociation in HAMMONIA, which would contribute to the bias in the modeled  $\text{O}_3$  sensitivity to the 27-day cycle. As shown in Figure 3, HAMMONIA also significantly underestimates the ozone secondary maximum and its semiannual variations. This suggests possible biases in the representation of dynamical and transport processes that affect the distribution of key reactive

constituents (e.g., O or H) and the temperature that influence the ozone distribution. Some of the model biases are meant to be implicitly accounting for in the scaling factor that is used to correct the HAMMONIA ozone sensitivity profile for the comparison with GOMOS results (Figure 8). Another possible cause of discrepancies between observations and model simulations is natural variability. Figure 5 illustrates that despite an idealized periodical 27-day solar forcing, the ozone response is very variable at this time scale. The internal variability can strongly contribute to modulate and/or mask the ozone solar signal (see, e.g., Thiéblemont et al., 2017) and thus constitutes an additional important source of uncertainty when the ozone response to 27-day solar rotational cycle is derived from short observed time series. Further sensitivity experiments and longer observed time series are required to assess the contributions of these uncertainty sources.

As already mentioned in section 2.2, the use of MSISE-90 temperature profiles to convert ozone number density observed by GOMOS to vmr may also be a source of uncertainty in the retrieving of ozone solar signal. For instance, Maycock et al. (2016) showed that the ozone response to the 11-year solar cycle derived from Stratospheric Aerosol and Gas Experiment II observations substantially depends on the representation of the temperature solar signal in reanalysis data sets that were used to convert number densities to vmr (in their case, comparing Modern Era Retrospective-Analysis for Research and Applications and National Centers for Environmental Prediction data sets). Similarly, misrepresented 27-day temperature solar signal in HAMMONIA, which is a pressure-based model, could affect the conversion of vertical profiles onto geometric altitude and hence induce altitude shifts. This could be a source of discrepancies between observed and model results. Our analysis of the MSISE-90 temperature profiles revealed no temperature response to the 27-day solar rotational cycle (not shown). Even though this is certainly related to the fact that the MSISE-90 model cannot represent completely the mesosphere/thermosphere subseasonal variability (Hedin, 1991), Sukhodolov et al. (2017) have shown that the temperature response to the 27-day cycle in the stratosphere/mesosphere remains weak (and thus difficult to detect) due to the largely dominating random internal variability at these time scales. This is consistent with the fact that the temperature response to the 27-day cycle in HAMMONIA is overall weak in the stratosphere and mesosphere (see Gruzdev et al., 2009). These results hence suggest that potential misrepresentations of the temperature response to the 27-day solar cycle in MSISE-90 and HAMMONIA have presumably a small influence on the observed ozone solar signal and should moderately affect the model/observation comparison. Nonetheless, an accurate quantification of this source of uncertainty would be required.

Finally, the model results show that semiannual variations modulate the upper mesospheric nighttime ozone response to solar rotational fluctuations. We find that the solar ozone anticorrelation and the magnitude of the ozone sensitivity are more pronounced  $\sim 3$  weeks after the minimum phase of the semiannual oscillation of ozone. This suggests that changes in the mean background state, associated with semiannual variations in the mesopause region, could lead to changes in the ozone response to the 27-day solar irradiance fluctuations by modifying the ozone equilibrium values. Moreover, seasonal changes in the amplitude of the internal dynamical variability may also have an effect on the ozone solar signal. The influence of semiannual variations on the ozone response to the 27-day solar cycle could, however, not be confirmed by the observations.

In conclusion, our results show that the mesospheric nighttime ozone significantly responds to solar short-term variations and that the magnitude of the response is particularly large in the upper MLT. More studies are required to assess the ability of models to simulate this ozone response that seems to be underestimated in the case of HAMMONIA. Such efforts will improve our understanding of the chemical and dynamical processes driving the middle atmosphere.

#### Acknowledgments

This project was supported by the European Project StratoClim (7th framework programme, grant agreement 603557) and the grant SOLSPEC from the Centre d'Etude Spatiale (CNES). R. T. was supported by a grant from the LABEX L-IPSL (ANR-10-LABX-0018), funded by the French Agence Nationale de la Recherche under the *Programme d'Investissements d'Avenir*. ENVISAT-GOMOS ozone data are available at <https://earth.esa.int/web/guest/-/gomos-level-2-atmospheric-constituents-profiles-1506> following registration. HAMMONIA ozone time series used in this study are publicly available at <https://figshare.com/s/67a1508c022c1227e291>. We thank the three anonymous referees for their detailed review comments, which improved the manuscript.

#### References

- Aikin, A., & Smith, H. (1986). Mesospheric ozone changes associated with 27 day solar ultraviolet flux variations. *Geophysical Research Letters*, 13(5), 427–430. <https://doi.org/10.1029/GL013i005p00427>
- Allen, M., Lunine, J., & Yung, Y. (1984). The vertical distribution of ozone in the mesosphere and lower thermosphere. *Journal of Geophysical Research*, 89(D3), 4841–4872. <https://doi.org/10.1029/JD089iD03p04841>
- Austin, J., Hood, L. L., & Soukharev, B. (2007). Solar cycle variations of stratospheric ozone and temperature in simulations of a coupled chemistry-climate model. *Atmospheric Chemistry and Physics*, 7(6), 1693–1706. <https://doi.org/10.5194/acp-7-1693-2007>
- Barth, C. A., Rusch, D. W., Thomas, D. W., Mount, G. H., Rottman, G. J., Thomas, G. E., et al. (1983). Solar mesospheric explorer: Scientific objectives and results. *Geophysical Research Letters*, 10(4), 237–240. <https://doi.org/10.1029/GL010i004p00237>
- Bertaux, J.-L., Kyrölä, E., Fussen, D., Hauchecorne, A., Dalaudier, F., Sofieva, V., et al. (2010). Global Ozone Monitoring by Occultation of Stars: An overview of GOMOS measurements on ENVISAT. *Atmospheric Chemistry and Physics*, 10(24), 12,091–12,148. <https://doi.org/10.5194/acp-10-12091-2010>

- Bossay, S., Bekki, S., Marchand, M., Poulain, V., & Toumi, R. (2015). Sensitivity of tropical stratospheric ozone to rotational UV variations during the declining phases of solar cycles 22 and 23. *Journal of Atmospheric and Solar - Terrestrial Physics*, 130-131, 96–111. <https://doi.org/10.1016/j.jastp.2015.05.014>
- Brasseur, G. (1993). The response of the middle atmosphere to long-term and short-term solar variability: A two-dimensional model. *Journal of Geophysical Research*, 98(D12), 23,079–23,090. <https://doi.org/10.1029/93JD02406>
- Brasseur, G., & Solomon, S. (1986). *Aeronomy of the middle atmosphere* (p. 452). Boston: D. Reidel. <https://doi.org/10.1007/978-94-009-4762-7>
- Chabrilat, S., & Kockarts, G. (1998). Correction to "Simple parameterization of the absorption of the solar Lyman-alpha line". *Geophysical Research Letters*, 25(1), 79–80. <https://doi.org/10.1029/97GL03569>
- Chandra, S., & McPeters, R. D. (1994). The solar cycle variation of ozone in the stratosphere inferred from Nimbus 7 and NOAA 11 satellites. *Journal of Geophysical Research*, 99(D10), 20,665–20,671. <https://doi.org/10.1029/94JD02010>
- Chen, L., London, J., & Brasseur, G. (1997). Middle atmosphere ozone and temperature responses to solar irradiance variations over 27-day periods. *Journal of Geophysical Research*, 102(D25), 29,957–29,979. <https://doi.org/10.1029/97JD02467>
- Dikty, S., Weber, M., von Savigny, C., Sonkaew, T., Rozanov, A., & Burrows, J. P. (2010). Modulations of the 27-day solar rotation signal in stratospheric ozone from scanning imaging absorption spectrometer for atmospheric cartography (SCIAMACHY) (2003–2008). *Journal of Geophysical Research*, 115, D00115. <https://doi.org/10.1029/2009JD012379>
- Ebisuzaki, W. A. (1997). Method to estimate the statistical significance of a correlation when the data are serially correlated. *Journal of Climate*, 10(9), 2147–2153. [https://doi.org/10.1175/1520-0442\(1997\)010<2147:AMTETS>2.0.CO;2](https://doi.org/10.1175/1520-0442(1997)010<2147:AMTETS>2.0.CO;2)
- Eckman, R. S. (1986). The response of ozone to short-term variations in the solar ultraviolet irradiance 2. Observations and interpretation. *Journal of Geophysical Research*, 91(D6), 6705–6721. <https://doi.org/10.1029/JD091iD06p06705>
- Fioletov, V. (2009). Estimating the 27-day and 11-year solar cycle variations in tropical upper stratospheric ozone. *Journal of Geophysical Research*, 114, D02302. <https://doi.org/10.1029/2008JD010499>
- Fleming, E. L., Chandra, S., Jackman, C. H., Considine, D. B., & Douglass, A. R. (1995). The middle atmospheric response to short and long term solar UV variations: Analysis of observations and 2D model results. *Journal of Atmospheric and Solar - Terrestrial Physics*, 57(4), 333–365. [https://doi.org/10.1016/0021-9169\(94\)E0013-D](https://doi.org/10.1016/0021-9169(94)E0013-D)
- Giorgetta, M. A., Manzini, E., Roeckner, E., Esch, M., & Bengtsson, L. (2006). Climatology and forcing of the QBO in MAECHAM5. *Journal of Climate*, 19(16), 3882–3901. <https://doi.org/10.1175/JCLI3830.1>
- Grenfell, J., Kunze, M., Langematz, U., Mieth, P., & Steil, B. (2010). The 27-day solar rotational cycle in the Freie Universität Berlin Climate Middle Atmosphere Model with interactive Chemistry (FUB CMAM CHEM). *Journal of Atmospheric and Solar - Terrestrial Physics*, 72(9–10), 705–712. <https://doi.org/10.1016/j.jastp.2010.03.012>
- Gruzdev, A., Schmidt, H., & Brasseur, G. (2009). The effect of the solar rotational irradiance variation on the middle and upper atmosphere calculated by a three-dimensional chemistry-climate model. *Atmospheric Chemistry and Physics*, 9(2), 595–614. <https://doi.org/10.5194/acp-9-595-2009>
- Haam, E., & Tung, K.-K. (2012). Statistics of solar cycle–La Niña connection: Correlation of two autocorrelated time series. *Journal of the Atmospheric Sciences*, 69(10), 2934–2939. <https://doi.org/10.1175/JAS-D-12-0101.1>
- Hedin, A. E. (1991). Extension of the MSIS thermosphere model into the middle and lower atmosphere. *Journal of Geophysical Research*, 96(A2), 1159–1172. <https://doi.org/10.1029/90JA02125>
- Hood, L., & Zhou, S. (1998). Stratospheric effects of 27-day solar ultraviolet variations: An analysis of UARS MLS ozone and temperature data. *Journal of Geophysical Research*, 103(D3), 3629–3638. <https://doi.org/10.1029/97JD02849>
- Hood, L. L. (1986). Coupled stratospheric ozone and temperature responses to short-term changes in solar ultraviolet flux: An analysis of NIMBUS 7 SBUV and SAMS data. *Journal of Geophysical Research*, 91(D4), 5264–5276. <https://doi.org/10.1029/JD091iD04p05264>
- Hood, L. L., Huang, Z., & Bougher, S. W. (1991). Mesospheric effects of solar ultraviolet variations: Further analysis of SME IR ozone and Nimbus 7 SAMS temperature data. *Journal of Geophysical Research*, 96(D7), 12,989–13,002. <https://doi.org/10.1029/91JD01177>
- Huang, F. T., Mayr, H. G., Russell, J. M., Mlynczak, M., & Reber, C. A. (2008). Ozone diurnal variations and mean profiles in the mesosphere, lower thermosphere, and stratosphere, based on measurements from SABER on TIMED. *Journal of Geophysical Research*, 113, A04307. <https://doi.org/10.1029/2007JA012739>
- Keating, G., Pitts, M., Brasseur, G. P., & De Rudder, A. (1987). Response of middle atmosphere to short-term solar ultraviolet variations: 1. Observations. *Journal of Geophysical Research*, 92(D1), 889–902.
- Kenesha, T. J., Zimmerman, S. P., & Philbrick, C. R. (1979). A dynamical model of the mesosphere and lower thermosphere. *Planetary and Space Science*, 27(4), 385–401. [https://doi.org/10.1016/0032-0633\(79\)90115-6](https://doi.org/10.1016/0032-0633(79)90115-6)
- Kinnison, D. E., Brasseur, G. P., Walters, S., Garcia, R. R., Marsh, D. R., Sassi, F., et al. (2007). Sensitivity of chemical tracers to meteorological parameters in the MOZART-3 chemical transport model. *Journal of Geophysical Research*, 112, D20302. <https://doi.org/10.1029/2006JD007879>
- Koppers, G. A. A., & Murtagh, D. P. (1996). Model studies of the influence of O<sub>2</sub> photodissociation parameterizations in the Schumann-Runge bands on ozone related photolysis in the upper atmosphere. *Annales de Geophysique*, 14, 68–79.
- Kyrölä, E., Tamminen, J., Leppelmeier, G. W., Sofieva, V., Hassinen, S., Seppälä, A., et al. (2006). Nighttime ozone profiles in the stratosphere and mesosphere by the Global Ozone Monitoring by Occultation of Stars on Envisat. *Journal of Geophysical Research*, 111, D24306. <https://doi.org/10.1029/2006JD007193>
- Kyrölä, E., Tamminen, J., Sofieva, V., Bertaux, J.-L., Hauchecorne, A., Dalaudier, F., et al. (2010b). GOMOS O<sub>3</sub>, NO<sub>2</sub>, and NO<sub>3</sub> observations in 2002–2008. *Atmospheric Chemistry and Physics*, 10(16), 7723–7738. <https://doi.org/10.5194/acp-10-7723-2010>
- Kyrölä, E., Tamminen, J., Sofieva, V., Bertaux, J.-L., Hauchecorne, A., Dalaudier, F., et al. (2010a). Retrieval of atmospheric parameter from GOMOS data. *Atmospheric Chemistry and Physics*, 10, 11,881–11,903.
- Madronich, S., & Flocke, S. (1999). The role of solar radiation in atmospheric chemistry. In *Environmental photochemistry* (pp. 1–26). Berlin: Springer.
- Manzini, E., Giorgetta, M. A., Esch, M., Kornbluh, L., & Roeckner, E. (2006). Sensitivity of the northern winter stratosphere to sea surface temperature variations: Ensemble simulations with the MAECHAM5 model. *Journal of Climate*, 19(16), 3863–3881. <https://doi.org/10.1175/JCLI3826.1>
- Maycock, A. C., Matthes, K., Tegtmeier, S., Thiéblemont, R., & Hood, L. (2016). The representation of solar cycle signals in stratospheric ozone—Part 1: A comparison of satellite observations. *Atmospheric Chemistry and Physics*, 16, 1–52. <https://doi.org/10.5194/acp-2015-882>
- Merkel, A. W., Harder, J. W., Marsh, D. R., Smith, A. K., Fontenla, J. M., & Woods, J. M. (2011). The impact of solar spectral irradiance variability on middle atmospheric ozone. *Geophysical Research Letters*, 38, L13802. <https://doi.org/10.1029/2011GL047561>
- Minschwaner, K., & Siskind, D. E. (1993). A new calculation of NO photolysis in the stratosphere, mesosphere, and lower thermosphere. *Journal of Geophysical Research*, 98(D11), 20,401–20,412. <https://doi.org/10.1029/93JD02007>

- Mudelsee, M. (2014). *Climate time series analysis: Classical statistical and bootstrap methods* (2nd ed.). Cham Heidelberg New York Dordrecht London: Springer. <https://doi.org/10.1007/978-3-319-04450-7>
- Pancheva, D., Mukhtarov, P., & Smith, A. K. (2014). Nonmigrating tidal variability in the SABER/TIMED mesospheric ozone. *Geophysical Research Letters*, *41*, 4059–4067. <https://doi.org/10.1002/2014GL059844>
- Rodrigo, R., Lopez-Moreno, J., Lopez-Puertas, M., Moreno, F., & Molina, A. (1986). Neutral atmospheric composition between 60 and 220 km: A theoretical model for mid-latitudes. *Planetary and Space Science*, *34*(8), 723–743. [https://doi.org/10.1016/0032-0633\(86\)90126-1](https://doi.org/10.1016/0032-0633(86)90126-1)
- Rodrigo, R., Nisbet, J., & Battaner, E. (1981). The effect of horizontal winds upon the chemical composition of the lower thermosphere at high latitude. *Journal of Geophysical Research*, *86*(A5), 3501–3508. <https://doi.org/10.1029/JA086iA05p03501>
- Roeckner, E., Bäuml, G., Bonaventura, L., Brokopf, R., Esch, M., Giorgetta, M., et al. (2003). The atmospheric general circulation model ECHAM 5. Part I: Model description. Technical Report 349, MPI for Meteorology, Hamburg, Germany.
- Roeckner, E., Brokopf, R., Esch, M., Giorgetta, M., Hagemann, S., Kornblueh, L., et al. (2006). Sensitivity of simulated climate to horizontal and vertical resolution in the ECHAM5 atmosphere model. *Journal of Climate*, *19*(16), 3771–3791. <https://doi.org/10.1175/JCLI3824.1>
- Roazanov, E., Egorova, T., Schmutz, W., & Peter, T. (2006). Simulation of the stratospheric ozone and temperature response to the solar irradiance variability during Sun rotation cycle. *Journal of Atmospheric and Solar - Terrestrial Physics*, *68*(18), 2203–2213. <https://doi.org/10.1016/j.jastp.2006.09.004>
- Ruzmaikin, A., Santee, M. L., Schwartz, M. J., Froidevaux, L., & Pickett, H. M. (2007). The 27-day variations in stratospheric ozone and temperature: New MLS data. *Geophysical Research Letters*, *34*, L02819. <https://doi.org/10.1029/2006GL028419>
- Schmidt, H., Brasseur, G. P., Charron, M., Manzini, E., Giorgetta, M. A., Diehl, T., et al. (2006). The HAMMONIA chemistry climate model: Sensitivity of the mesopause region to the 11-year solar cycle and CO<sub>2</sub> doubling. *Journal of Climate*, *19*(16), 3903–3931. <https://doi.org/10.1175/JCLI3829.1>
- Shapiro, A., Roazanov, E., Shapiro, A., Wang, S., Egorova, T., Schmutz, W., & Peter, T. (2012). Signature of the 27-day solar rotation cycle in mesospheric OH and H<sub>2</sub>O observed by the Aura Microwave Limb Sounder. *Atmospheric Chemistry and Physics*, *12*(7), 3181–3188. <https://doi.org/10.5194/acp-12-3181-2012>
- Shimazaki, T., & Laird, A. (1970). A model calculation of the diurnal variation in minor neutral constituents in the mesosphere and lower thermosphere including transport effects. *Journal of Geophysical Research*, *75*(16), 3221–3235. <https://doi.org/10.1029/JA075i016p03221>
- Smith, A. K., Harvey, V. L., Mlynarczyk, M. G., Funke, B., García-Comas, M., Hervig, M., et al. (2013). Satellite observations of ozone in the upper mesosphere. *Journal of Geophysical Research: Atmospheres*, *118*, 5803–5821. <https://doi.org/10.1002/jgrd.50445>
- Smith, A. K., López-Puertas, M., Funke, B., García-Comas, M., Mlynarczyk, M. G., & Holt, L. A. (2015). Nighttime ozone variability in the high latitude winter mesosphere. *Journal of Geophysical Research: Atmospheres*, *119*, 13,547–13,564. <https://doi.org/10.1002/2014JD021987>
- Smith, A. K., & Marsh, D. R. (2005). Processes that account for the ozone maximum at the mesopause. *Journal of Geophysical Research*, *110*, D23305. <https://doi.org/10.1029/2005JD006298>
- Smith, A. K., Marsh, D. R., Russell, J. M. III, Mlynarczyk, M. G., Martin-Torres, F. J., & Kyrölä, E. (2008). Satellite observations of high nighttime ozone at the equatorial mesopause. *Journal of Geophysical Research*, *113*, D17312. <https://doi.org/10.1029/2008JD010066>
- Sofieva, V. F., Vira, J., Kyrölä, E., Tamminen, J., Kan, V., Dalaudier, F., et al. (2010). Retrievals from GOMOS stellar occultation measurements using characterization of modeling errors. *Atmospheric Measurement Techniques*, *3*, 1019–1027. <https://doi.org/10.5194/amt-3-1019-2010>
- Sukhodolov, T., Roazanov, E., Ball, W. T., Peters, T., & Schmutz, W. (2017). Modeling of the middle atmosphere response to 27-day solar irradiance variability. *Journal of Atmospheric and Solar - Terrestrial Physics*, *152–153*, 50–61.
- Thiéblemont, R., Marchand, M., Bekki, S., Bossay, S., Meftah, M., & Hauchecorne, A. (2017). Sensitivity of the tropical stratospheric ozone response to the solar rotational cycle in observations and chemistry-climate model simulations. *Atmospheric Chemistry and Physics*, *17*(16), 9897–9916. <https://doi.org/10.5194/acp-17-9897-2017>
- Thuillier, G., Deland, M., Shapiro, A., Schmutz, W., Bolsée, D., & Melo, S. M. L. (2012). The solar spectral irradiance as a function of the Mg II index for atmosphere and climate modelling. *Solar Physics*, *277*(2), 245–266. <https://doi.org/10.1007/s11207-011-9912-5>
- Thuillier, G., Melo, S. M. L., Lean, J., Krivova, N. A., Bolduc, C., Fomichev, V. I., et al. (2014). Analysis of different solar spectral irradiance reconstructions and their impact on solar heating rates. *Solar Physics*, *289*(4), 1115–1142. <https://doi.org/10.1007/s11207-013-0381-x>
- Torrence, C., & Compo, G. P. (1998). A practical guide to wavelet analysis. *Bulletin of the American Meteorological Society*, *79*(1), 61–78. [https://doi.org/10.1175/1520-0477\(1998\)079<0061:APGTWA>2.0.CO;2](https://doi.org/10.1175/1520-0477(1998)079<0061:APGTWA>2.0.CO;2)
- Vaughan, G. (1984). Mesospheric ozone—Theory and observation. *Quarterly Journal of the Royal Meteorological Society*, *110*, 239–260.
- Williams, J., Austin, J., & Haigh, J. (2001). Model simulations of the impact of the 27-day solar rotation period on the stratosphere. *Advances in Space Research*, *27*(12), 1933–1942. [https://doi.org/10.1016/S0273-1177\(01\)00263-0](https://doi.org/10.1016/S0273-1177(01)00263-0)
- Zhou, S., Miller, A. J., & Hood, L. L. (2000). A partial correlation analysis of the stratospheric ozone response to 27-day solar UV variations with temperature effect removed. *Journal of Geophysical Research*, *105*(D4), 4491–4500. <https://doi.org/10.1029/1999JD901082>
- Zhou, S., Rottman, G. J., & Miller, A. J. (1997). Stratospheric ozone response to short- and intermediate-term variations in solar UV flux. *Journal of Geophysical Research*, *102*(D7), 9003–9011. <https://doi.org/10.1029/96JD03383>